Monthly Notices
of the
ROYAL ASTRONOMICAL SOCIETY

MNRAS **486,** 2947–2963 (2019) doi:10.1093/mnras/stz445
Advance Access publication 2019 February 25

Formation of the Cassini Division – II. Possible histories of Mimas and Enceladus

B. Noyelles [1,2★] K. Baillié,[3,4★] S. Charnoz,[5] V. Lainey[3,6] and G. Tobie[7]

[1]*NAmur Institute for CompleX SYStems (NAXYS), University of Namur, Rempart de la Vierge 8, B-5000 Namur, Belgium*
[2]*Institut UTINAM, CNRS UMR 6213, Univ. Bourgogne Franche-Comté, OSU THETA, BP 1615, F-25010 Besançon Cedex, France*
[3]*IMCCE, Observatoire de Paris, PSL Research University, CNRS, Sorbonne Universités, UPMC Univ Paris 06, Univ. Lille, 77 Av. Denfert-Rochereau, F-75014 Paris, France*
[4]*Centre National d'Études Spatiales (CNES), France*
[5]*Institut de Physique du Globe, Sorbonne Paris Cité, Université Paris Diderot/CNRS, 1 rue Jussieu, F-75005 Paris, France*
[6]*Jet Propulsion Laboratory, California Institute of Technology, 4800 Oak Grove Drive, Pasadena, CA 91109, USA*
[7]*Laboratoire de Planétologie et Géodynamique, Université de Nantes, CNRS, UMR-6112, BP 92208, 44322 Nantes Cedex 3, France*

Accepted 2019 February 7. Received 2018 December 18; in original form 2018 April 27

ABSTRACT

This study is a companion paper to Baillié et al., in which we showed that a past episode of inward migration of Mimas could have created the Cassini Division. We here investigate the possible causes of this inward migration. We suggest two scenarios: one based on a past intense heating of Mimas, and another one on a past intense heating of Enceladus, which would have itself driven an inward migration of Mimas due to a mean-motion resonance. These two scenarios are challenged with numerical modelling of the orbital motion of the satellites, and energy budget, which are confronted to our present knowledge of the interior of Mimas and Enceladus. We show that a past hot Mimas requires an eccentricity of 0.22, while a past hot Enceladus would have needed an eccentricity of 0.25. While the scenario of a past hot Mimas preserves the stability of the mid-sized satellites of Saturn, it threatens Janus and Epimetheus and is inconsistent with the observations of impact basins at the surface of Mimas. However, a past hot Enceladus which would have almost fully melted could be consistent with its differentiated interior, but would probably not have preserved the stability of Tethys, given the high eccentricity required. Both of these scenarios would have challenged the stability of Aegaeon, Methone, Pallene, and Anthe, and implied that the Cassini Division would be younger than 10 Myr.

Key words: methods: numerical – celestial mechanics – planets and satellites: individual: Saturn.

1 INTRODUCTION

In Baillié et al. (2019), hereafter called *Paper I*, we have shown that a past inward migration of Mimas over at least 8000 km in a few Myr would explain the creation of the Cassini Division, implying that this division is a transient structure, which should disappear in ≈40 Myr. This companion paper tackles the issue of the possible origin of an inward migration of Mimas.

In systems of planetary satellites, an episode of inward migration is usually attributed to an intense dissipation in a satellite, which outweighs the dissipation in the planet. This dissipation would have consequences for the geophysical activity of the satellite, which would now present evidence of this active episode. In the system of Saturn, Mimas does not present obvious signature of such past activity, while Enceladus appears to be much more active.

After describing some aspects of the dynamics of the system of Saturn (Section 2), we will present the secular torque of the rings (Section 3) and the tidal torque (Section 4). Then we will describe our methodology (Section 5), which consists both of the use of synthetic trajectories and *N*-body integrations. Then we will investigate two scenarios: one based on an initially hot Mimas (Section 6), and the other one based on an initially hot Enceladus (Section 7), before discussing their consequences on the stability of the other satellites of the Saturnian system (Section 8).

★ E-mail: benoit.noyelles@univ-fcomte.fr (BN); kevin.baillie@obspm.fr (KB)

2 THE PRESENT SYSTEM OF SATURN

This study presents putative histories of the system of Saturn, which must be consistent with its observed state. The mid-sized satellites, i.e. S-1 Mimas, S-2 Enceladus, S-3 Tethys, and S-4 Dione, have the richest orbital dynamics. We recall their orbital elements in Table 1.

(i) Mimas is in a 4: 2 mean motion resonance (MMR) with Tethys, which excites its inclination. The high libration amplitude of its resonant argument ($\approx 97^\circ$, Struve 1890) suggests a recent capture. Allan (1969) estimated its age to be $3345/(k_2/Q)_Y$ yr in neglecting the dissipation in Mimas, which evaluates to 21 Myr if we adopt the recent measurement of the dissipative Love number of Saturn $(k_2/Q)_Y$ by Lainey et al. (2017). Mimas also has a significant eccentricity (0.02), which could be due to several crossings of mean-motion resonances (Meyer & Wisdom 2008). Even if its surface appears old and frozen, recent measurements of longitudinal librations in its rotational dynamics (Tajeddine et al. 2014) are consistent with the presence of a subsurface ocean. Not only the amplitude of libration is probably too high for a frozen body, but its phase lag ($6.35 \pm 0.8^\circ$) is the signature of a significant internal dissipation (Caudal 2017; Noyelles 2017).

(ii) Enceladus is in a 2: 1 MMR with Dione, which excites its eccentricity. The observations of jets of water vapour and icy grains at its South Pole (Porco et al. 2006; Howett et al. 2011), the relaxation of the craters (Bland et al. 2012), the detection of a global ocean (Thomas et al. 2016) as well as an ice shell thinning at the South Pole (Beuthe, Rivoldini & Trinh 2016; Čadek et al. 2016) associated with a strong heat flow anomaly (Le Gall et al. 2017) suggest that intense dissipation is currently taking place in Enceladus.

(iii) Tethys does not exhibit any sign of recent activity (Buratti et al. 2011). It has a significant inclination ($\approx 1^\circ$), which cannot be explained by the resonance with Mimas, given their mass ratio. A recent study (Ćuk, Dones & Nesvorný 2016) identifies a former secular resonance with Dione as a possible cause for this inclination.

The larger outer satellites, i.e. Rhea, Titan, Hyperion, and Iapetus, can be safely neglected. They induce a small contribution in the secular precessions of the nodes and pericentres, which is negligible compared to the influence of Saturn's flattening.

Most interesting are the inner satellites on which Mimas and Enceladus have a critical influence. Their existence could be threatened by any dramatic change in the orbits of Mimas and Enceladus, so they should either survive the proposed scenario of orbital evolution, or have been formed very recently. The main satellites to look for are Janus, Epimetheus, Aegaeon, Anthe, and Pallene. Janus and Epimetheus are two coorbital satellites, i.e. sharing the same orbit. Aegaeon orbits within a bright arc of material near the inner edge of the G-ring, and is in a 7: 6 MMR with Mimas (Hedman et al. 2010). Methone, Anthe, and Pallene are the Alkyonides satellites; they are in the 15: 14 (Spitale et al. 2006) and 11: 10 (Cooper et al. 2008) MMR with Mimas, and 19: 16 MMR with Enceladus (Spitale et al. 2006), respectively. We recall their orbital elements in Table 2.

Moreover, Mimas is known to exert Lindblad resonances across the rings. The first-order 2: 1 resonance is located at the inner edge of the Cassini Division and its influence on the shaping of the Division is debated in Paper I. However, higher order Lindblad resonances have also been noticed to create signatures and structures across the rings such as the Mimas 4: 1 inner Lindblad resonance reported in Baillié et al. (2011). Though located close to the edge separating the C ring and the B ring, the Mimas 3: 1 has not been positively associated with any ring structure yet. The difference between the C ring and the Cassini Division, which yet present similar optical depth, may be due to possible different origins of the ring particles between these rings as suggested by particle size distribution analyses by French & Nicholson (2000) and Baillié et al. (2013).

3 THE PUSH OF THE RINGS

From Goldreich & Tremaine (1980), Champenois (1998, Chapter 3) shows that the push exerted by the rings of Saturn on Mimas mostly comes from the 2: 1 Lindblad resonance, and the resulting secular variation of the mean motion reads

$$\frac{\mathrm{d}n_1}{\mathrm{d}t} = -2\pi^2 \sigma_{2:1} n_1^2 a_1^2 \alpha^3 \frac{m_1}{M_Y^2} \left(4b_{1/2}^{(2)}(\alpha) + \alpha \frac{\mathrm{d}b_{1/2}^{(2)}}{\mathrm{d}\alpha}(\alpha) \right)^2, \tag{1}$$

where $\alpha = 2^{-2/3} \approx 0.63$ is the ratio of the semimajor axes of the 2: 1 Lindblad resonance and Mimas, and $\sigma_{2:1}$ is the density of the rings at this resonance. Baillié et al. (2011) and Hedman & Nicholson (2016) provide estimations of the ring density at various locations in the rings corresponding to specific resonances with outer satellites. $b_{1/2}^{(2)}(\alpha)$ is a classical Laplace coefficient, which reads:

$$b_{1/2}^{(2)}(\alpha) = \frac{2}{\pi} \int_0^\pi \frac{\cos 2\phi}{\sqrt{1 - 2\alpha \cos\phi + \alpha^2}} \mathrm{d}\phi. \tag{2}$$

4 TIDES IN THE SYSTEM OF SATURN

Tidal interaction can be a major source of energy through internal friction in planetary satellites, and is responsible for their secular migration. The relevant equations are (e.g. Yoder & Peale 1981)

$$\frac{\mathrm{d}n_i}{\mathrm{d}t} = -\frac{9}{2} \left(\frac{k_2}{Q} \right)_Y n_i^2 \frac{m_i}{M_Y} \left(\frac{R_Y}{a_i} \right)^5 \left(1 + \frac{51}{4} e_i^2 \right) + \frac{63}{2} \left(\frac{k_2}{Q} \right)_i n_i^2 \frac{M_Y}{m_i} \left(\frac{R_i}{a_i} \right)^5 e_i^2, \tag{3}$$

$$\frac{\mathrm{d}e_i}{\mathrm{d}t} = \frac{57}{8}\left(\frac{k_2}{Q}\right)_Y n_i \frac{m_i}{M_Y}\left(\frac{R_Y}{a_i}\right)^5 e_i - \frac{21}{2}\left(\frac{k_2}{Q}\right)_i n_i \frac{M_Y}{m_i}\left(\frac{R_i}{a_i}\right)^5 e_i, \tag{4}$$

for a small eccentricity e_i, a synchronous rotation of the satellite, and an orbital period which is larger than the rotation period of the planet. Here n_i is the orbital frequency of the satellite i, m_i its mass, R_i its radius, and a_i its semimajor axis. R_Y and M_Y are the mean radius and the mass of Saturn, respectively. k_2 and Q are the Love number and the dissipation factor, in Saturn (subscript Y) and in the satellite i. The raise of the eccentricity of the satellite would not be enough to destabilize the synchronous rotation.

Lainey et al. (2017) measured $(k_2/Q)_Y = (1.59 \pm 0.74) \times 10^{-4}$ for the whole system of Saturn. An investigation of the dependency of $(k_2/Q)_Y$ on the orbital frequency suggests that the dissipation increases when the frequency decreases, in particular the same study found $(k_2/Q)_Y = (1.2394 \pm 0.1727) \times 10^{-3}$ at Rhea's frequency. This could be the first observational confirmation of the resonance locking predicted by Fuller, Luan & Quataert (2016). This mechanism consists of a high dissipation in the atmosphere of the planet at a very specific frequency, but which evolves with the orbit of a given satellite, so that the satellite experiences a large migration rate all along its migration process, except if a catastrophic event disrupts this resonance.

We can notice that the secular migration of a planetary satellite is driven by opposite phenomena:

(i) the dissipation in the planet is responsible for the outward migration of satellites ($\mathrm{d}n_i/\mathrm{d}t < 0$),
(ii) this effect is supplemented by the push of the rings, while
(iii) the dissipation in the satellite translates into a loss of orbital energy, i.e. an inward migration ($\mathrm{d}n_i/\mathrm{d}t > 0$).

This assumes that the only gravitational action which does not average to zero is the tides. Actually, when two satellites are trapped in a mean-motion resonance, energy exchanges between them result in a joint migration. A consequence is that a satellite can migrate inwards because another one is dissipating.

This allows us to identify two possible causes for an inward migration of Mimas:

(i) A past intense dissipation in Mimas,
(ii) A past intense dissipation in another satellite, which would be locked in mean-motion resonance with Mimas and drive it inwards.

It could also be a combination of both processes. For the sake of simplicity, we will consider these two scenarios separately here.

An intense dissipation in a satellite should be the consequence of an intense heating. In this study we will assume that this heating results from an increase of the eccentricity. A higher eccentricity results in a higher tidal heating, which would tend to melt the satellite and elevate $(k_2/Q)_i$, which would itself trigger an inward migration. During the migration process, the eccentricity would be damped, eventually stopping the dissipation in the satellite and reversing the migration outwards.

5 METHODOLOGY

To investigate the long-term dynamics of the satellites of Saturn, we will essentially use two tools: a full N-body integrator and an analytical theory of the orbital evolution of satellites in resonance. The analytical evolution gives us trajectories of the satellites very efficiently, while the N-body integrator checks their validity in a realistic system.

5.1 Secular and resonant orbital motion

Over Gyr time-scales, the orbital variations of the satellites are mainly due to tides and resonant interactions. Resonant interactions originate from mean-motion resonances between two bodies, and result in a pair which migrates with a stable semimajor axial ratio, and some orbital elements, i.e. eccentricities and / or inclinations, of one or of the two satellites, which are raised. To represent this evolution, we will average the equations that determine the variation of the relevant orbital elements over time, to only keep the secular and resonant contributions. This model is widely inspired from the PhD dissertation of Sylvain Champenois (Champenois 1998, Chapter 4), which has been itself inspired by Allan (1969).

When a satellite is disturbed by an external potential U, then the time evolution of its orbital elements is determined by the classical Lagrange equations:

$$\frac{\mathrm{d}n}{\mathrm{d}t} = -\frac{3}{a^2}\frac{\partial U}{\partial \lambda}, \tag{5}$$

$$\frac{\mathrm{d}e}{\mathrm{d}t} = -\frac{\sqrt{1-e^2}}{na^2 e}\left(1-\sqrt{1-e^2}\right)\frac{\partial U}{\partial \lambda} - \frac{\sqrt{1-e^2}}{na^2 e}\frac{\partial U}{\partial \varpi}, \tag{6}$$

$$\frac{\mathrm{d}I}{\mathrm{d}t} = -\frac{\tan(I/2)}{na^2\sqrt{1-e^2}}\left(\frac{\partial U}{\partial \lambda} + \frac{\partial U}{\partial \varpi}\right) - \frac{1}{na^2\sqrt{1-e^2}\sin I}\frac{\partial U}{\partial e}, \tag{7}$$

$$\frac{\mathrm{d}\lambda}{\mathrm{d}t} = n - \frac{2}{na}\frac{\partial U}{\partial a} + \frac{\sqrt{1-e^2}}{na^2 e}\left(1-\sqrt{1-e^2}\right)\frac{\partial U}{\partial e} + \frac{\gamma}{2na^2\sqrt{1-e^2}}\frac{\partial U}{\partial \gamma}, \tag{8}$$

$$\frac{\mathrm{d}\varpi}{\mathrm{d}t} = \frac{\sqrt{1-e^2}}{na^2 e}\frac{\partial U}{\partial e} + \frac{\gamma}{2na^2\sqrt{1-e^2}}\frac{\partial U}{\partial \gamma}, \tag{9}$$

$$\frac{\mathrm{d}\Omega}{\mathrm{d}t} = \frac{1}{4na^2\gamma\sqrt{1-e^2}}\frac{\partial U}{\partial \gamma}, \tag{10}$$

with $\gamma = \sin(I/2)$.

The disturbing potentials U_1 and U_2 can be expanded with respect to the small eccentricities and inclinations e_1, e_2, γ_1, and γ_2 as a sum involving six integer indices l, m, s, s', t, t', as Kaula (1962, e.g.):

$$U = \sum_{lmss'tt'} \frac{\mathcal{G}M_Y}{a_2} F_{lmss'tt'} \cos\phi_{lmss'tt'}, \tag{11}$$

with

$$\phi_{lmss'tt'} = (l-2s+t)\lambda_1 - (l-2s'+t')\lambda_2 - (l-m-2s)\Omega_1 + (l-m-2s')\Omega_2 - t\varpi_1 + t'\varpi_2, \tag{12}$$

and $F_{lmss'tt'}$ is a function of the orbital elements verifying

$$F_{lmss'tt'} \propto e_1^{|t|} e_2^{|t'|} \gamma_1^{|l-m-2s|} e_2^{|l-m-2s'|}. \tag{13}$$

If we assume a $(p+q)$: p mean-motion resonance between Satellites 1 and 2, then the resonant argument ϕ reads

$$\phi = p\lambda_1 - (p+q)\lambda_2 + q_1\varpi_1 + q_2\varpi_2 + q_3\Omega_1 + q_4\Omega_2, \tag{14}$$

where λ_i, ϖ_i, and Ω_i are the mean longitudes, the longitudes of the pericentres, and of the ascending nodes of Satellite i, respectively. p, q, q_1, q_2, q_3, and q_4 are integers such that $q = q_1 + q_2 + q_3 + q_4$ and $q_3 + q_4$ are even.

After averaging over the non-resonant angles, only the resonant argument is kept in the disturbing potential, and the Lagrange equations yield:

$$\frac{\mathrm{d}n_1}{\mathrm{d}t} = 3pn_1^2\alpha\frac{m_2}{M_Y} e_1^{|q_1|} e_2^{|q_2|} \gamma_1^{|q_3|} \gamma_2^{|q_4|} f(\alpha)\sin\phi + \left(\frac{\mathrm{d}n_1}{\mathrm{d}t}\right)_T + \left(\frac{\mathrm{d}n_1}{\mathrm{d}t}\right)_R, \tag{15}$$

$$\frac{\mathrm{d}n_2}{\mathrm{d}t} = -3(p+q)n_2^2\frac{m_1}{M_Y} e_1^{|q_1|} e_2^{|q_2|} \gamma_1^{|q_3|} \gamma_2^{|q_4|} f(\alpha)\sin\phi + \left(\frac{\mathrm{d}n_2}{\mathrm{d}t}\right)_T, \tag{16}$$

$$\frac{\mathrm{d}e_1}{\mathrm{d}t} = n_1\alpha\frac{m_2}{M_Y}\left(q_1 + p\left(1-\sqrt{1-e_1^2}\right)\right)\sqrt{1-e_1^2} e_1^{|q_1|-1} e_2^{|q_2|} \gamma_1^{|q_3|} \gamma_2^{|q_4|} f(\alpha)\sin\phi + \left(\frac{\mathrm{d}e_1}{\mathrm{d}t}\right)_T, \tag{17}$$

$$\frac{\mathrm{d}e_2}{\mathrm{d}t} = n_2\frac{m_1}{M_Y}\left(q_2 + p\left(1-\sqrt{1-e_2^2}\right)\right)\sqrt{1-e_2^2} e_1^{|q_1|} e_2^{|q_2|-1} \gamma_1^{|q_3|} \gamma_2^{|q_4|} f(\alpha)\sin\phi + \left(\frac{\mathrm{d}e_2}{\mathrm{d}t}\right)_T, \tag{18}$$

$$\frac{\mathrm{d}I_1}{\mathrm{d}t} = \frac{n_1\alpha m_2}{2M_Y\cos(I_1/2)\sqrt{1-e_1^2}}\left(q_3 + 2(p+q_1)\gamma_1^2\right) e_1^{|q_1|} e_2^{|q_2|} \gamma_1^{|q_3|-1} \gamma_2^{|q_4|} f(\alpha)\sin\phi, \tag{19}$$

$$\frac{\mathrm{d}I_2}{\mathrm{d}t} = \frac{n_2 m_1}{2M_Y\cos(I_2/2)\sqrt{1-e_2^2}}\left(q_4 + 2(q_2-p-q)\gamma_2^2\right) e_1^{|q_1|} e_2^{|q_2|} \gamma_1^{|q_3|} \gamma_2^{|q_4|-1} f(\alpha)\sin\phi, \tag{20}$$

$$\begin{aligned}\frac{\mathrm{d}\lambda_1}{\mathrm{d}t} = {} & n_1 + n_1\frac{m_2}{M_Y}\alpha\left(-2\alpha\frac{\partial f}{\partial\alpha} + \sqrt{1-e_1^2}\left(|q_1|(1-\sqrt{1-e_1^2}) + |q_3|\frac{e_1^2}{2(1-e_1^2)}\right) f(\alpha)\right) \\ & \times e_1^{|q_1|} e_2^{|q_2|} \gamma_1^{|q_3|} \gamma_2^{|q_4|} f(\alpha)\cos\phi + \left(\frac{\mathrm{d}\lambda_1}{\mathrm{d}t}\right)_S,\end{aligned} \tag{21}$$

$$\begin{aligned}\frac{\mathrm{d}\lambda_2}{\mathrm{d}t} = {} & n_2 + n_2\frac{m_1}{M_Y}\left(2\left(f(\alpha)+\alpha\frac{\partial f}{\partial\alpha}\right) + \sqrt{1-e_2^2}\left(|q_2|(1-\sqrt{1-e_2^2}) + |q_4|\frac{e_2^2}{2(1-e_2^2)}\right) f(\alpha)\right) \\ & \times e_1^{|q_1|} e_2^{|q_2|} \gamma_1^{|q_3|} \gamma_2^{|q_4|} f(\alpha)\cos\phi + \left(\frac{\mathrm{d}\lambda_2}{\mathrm{d}t}\right)_S,\end{aligned} \tag{22}$$

$$\frac{\mathrm{d}\varpi_1}{\mathrm{d}t} = n_1\alpha\frac{m_2}{M_Y}\left(|q_1| + |q_3|\frac{e_1^2}{2(1-e_1^2)}\right) f(\alpha) e_1^{|q_1|-2} e_2^{|q_2|}\gamma_1^{|q_3|}\gamma_2^{|q_4|} f(\alpha)\cos\phi + \left(\frac{\mathrm{d}\varpi_1}{\mathrm{d}t}\right)_S, \tag{23}$$

$$\frac{\mathrm{d}\varpi_2}{\mathrm{d}t} = n_2\frac{m_1}{M_Y}\left(|q_2| + |q_4|\frac{e_2^2}{2(1-e_2^2)}\right) f(\alpha) e_1^{|q_1|} e_2^{|q_2|-2}\gamma_1^{|q_3|}\gamma_2^{|q_4|} f(\alpha)\cos\phi + \left(\frac{\mathrm{d}\varpi_2}{\mathrm{d}t}\right)_S, \tag{24}$$

$$\frac{\mathrm{d}\Omega_1}{\mathrm{d}t} = n_1\alpha\frac{m_2}{M_Y}\frac{|q_3|}{4\sqrt{1-e_1^2}} f(\alpha) e_1^{|q_1|} e_2^{|q_2|}\gamma_1^{|q_3|-2}\gamma_2^{|q_4|} f(\alpha)\cos\phi + \left(\frac{\mathrm{d}\Omega_1}{\mathrm{d}t}\right)_S, \tag{25}$$

$$\frac{\mathrm{d}\Omega_2}{\mathrm{d}t} = n_2\frac{m_1}{M_Y}\frac{|q_4|}{4\sqrt{1-e_2^2}} f(\alpha) e_1^{|q_1|} e_2^{|q_2|}\gamma_1^{|q_3|}\gamma_2^{|q_4|-2} f(\alpha)\cos\phi + \left(\frac{\mathrm{d}\Omega_2}{\mathrm{d}t}\right)_S, \tag{26}$$

with $\alpha = a_1/a_2 < 1$.

The subscripts T, R, and S refer to the tides, the rings, and to the secular conservative variations, respectively. Tides are expected to have a very small influence on the inclinations, which is why we neglect the quantities $(\mathrm{d}I_i/\mathrm{d}t)_T$. The secular variations of the angles λ, ϖ, and Ω are mostly due to the flattening of Saturn.

Since the precessions of the nodes and pericentres are very slow with respect to the mean motions n_i, we can write

$$\begin{aligned}\ddot{\phi} &\approx p\frac{\mathrm{d}n_1}{\mathrm{d}t} - (p+q)\frac{\mathrm{d}n_2}{\mathrm{d}t}\\ &\approx \left(3p^2n_1^2\alpha\frac{m_2}{M_Y} + 3(p+q)^2n_2^2\frac{m_1}{M_Y}\right) e_1^{|q_1|} e_2^{|q_2|}\gamma_1^{|q_3|}\gamma_2^{|q_4|} f(\alpha)\sin\phi\\ &\quad + p\left(\frac{\mathrm{d}n_1}{\mathrm{d}t}\right)_T + p\left(\frac{\mathrm{d}n_1}{\mathrm{d}t}\right)_R - (p+q)\left(\frac{\mathrm{d}n_2}{\mathrm{d}t}\right)_T,\end{aligned} \tag{27}$$

and since it follows from the resonance that ϕ librates, we have $<\ddot{\phi}>=0$, $<x>$ being the average of the quantity x over a period of variations. This yields

$$< e_1^{|q_1|} e_2^{|q_2|}\gamma_1^{|q_3|}\gamma_2^{|q_4|} f(\alpha)\sin\phi >= \frac{(p+q)\left(\frac{\mathrm{d}n_2}{\mathrm{d}t}\right)_T - p\left[\left(\frac{\mathrm{d}n_1}{\mathrm{d}t}\right)_T + \left(\frac{\mathrm{d}n_1}{\mathrm{d}t}\right)_R\right]}{3p^2n_1^2\alpha\frac{m_2}{M_Y} + 3(p+q)^2n_2^2\frac{m_1}{M_Y}}, \tag{28}$$

which can then be used in the Lagrange equations to express the evolution of the orbital elements over long time-scales.

This study requires eccentricities up to 0.25, which challenges the accuracy of this analytical representation. This is why we will confront it with full N-body simulations. However, the analytical representation has the advantage to show which mechanism, i.e. the MMR, is responsible for the eccentricity of Mimas. This is necessary for a preliminary exploration of the initial conditions and parameters. An attempt to make it convergent in adding higher order terms would prejudice this goal.

5.2 Full *N*-body integrator

We model the motion of the main satellites of Saturn in a Cartesian planetocentric reference frame, and consider the perturbations of N satellites seen as point masses, and the spherical harmonics (Stokes coefficients) J_2, J_4, and J_6 of the gravity field of Saturn. We give the required numbers in Table 3. In practice, we limit the integrations to $N = 4$, the involved satellites being Mimas, Enceladus, Tethys, and Dione. Even if Rhea and Titan are the most massive ones, numerical tests have shown that they have only limited influence on the dynamics of Mimas and Enceladus.

In this framework, the equations of the problem are

$$\ddot{\vec{r}}_i = \frac{\vec{F}_i}{m_i} - \frac{\vec{F}_p}{M_Y}, \tag{29}$$

where $\vec{r}_i = (x_i, y_i, z_i)$ locates the satellite i, m_i being its mass, $\vec{F}_i$ the force acting on it, and $\vec{F}_p$ the force acting on Saturn. We write the general equations of motion for the N satellites as

$$\ddot{\vec{r}}_i = -\frac{\mathcal{G}(M_Y + m_i)}{r_i^3}\vec{r}_i + \sum_{j=1, j\neq i}^{N}\mathcal{G}m_j\left(\frac{\vec{r}_j - \vec{r}_i}{r_{ij}^3} - \frac{\vec{r}_j}{r_i^3}\right) + \mathcal{G}M_Y\nabla_i U_i, \tag{30}$$

with

$$U_i = -\sum_{n=1}^{3}\frac{R_e^{2n}}{r_i^{2n+1}} J_{2n} P_{2n}(\sin\phi_i), \tag{31}$$

$\mathcal{G}$ being the gravitational constant, R_e the equatorial radius of Saturn, ϕ_i the latitude of the satellite i in a frame connected to Saturn, and P_n the classical Legendre polynomial. As in Verheylewegen, Noyelles & Lemaitre (2013), the tidal effects, given by equations (3) and (4),

are added on the orbital osculating elements derived from the Cartesian coordinates, these orbital elements being then converted back into Cartesian elements.

We have then numerically integrated the equations of motion of the *N*-body problem and of the tides with the Adams–Bashforth–Moulton 10th-order predictor-corrector integrator (Hairer, Nørsett & Wanner 1993). This integrator has been successfully validated in comparing it with SWIFT (Levison & Duncan 1994), in a similar study on the satellites of Uranus (Verheylewegen et al. 2013).

6 SCENARIO I: FROM A HOT MIMAS

Assuming Mimas has been hot enough to trigger inward migration, we consider the following scenario:

(i) The satellites of Saturn migrate outwards, with $\alpha_{13} = a_1/a_3 < 0.63107$. This ratio increases with time.

(ii) At $\alpha_{13} = 0.63107$, the system Mimas–Tethys encounters the resonance, whose argument is $\phi_1 = \lambda_1 - 2\lambda_3 + \varpi_1$, with $p = q = 1$. This resonance raises the eccentricity of Mimas.

(iii) When the internal temperature of Mimas reaches the melting point of water ice, the production of melt and the subsequent formation of an internal ocean leads to a dramatic increase of its dissipation function $(k_2/Q)_i$. As a consequence, the MMR with Tethys is disrupted, Mimas migrates inwards, and its eccentricity is damped.

(iv) The orbit of Mimas is now almost circular and migrates outwards. While Mimas is cooling, the quantity α_{13} increases until it reaches 0.62930. At this point, Mimas and Tethys are trapped into the present 4: 2 MMR, whose resonant argument is $\phi_2 = 2\lambda_1 - 4\lambda_3 + \Omega_1 + \Omega_3$, with $p = q = 2$.

The time-scale for eccentricity increase before runaway melting occurs is mostly controlled by the dissipation rate in Saturn and takes a few hundreds of Myr, while the time-scale for eccentricity damping is determined by the dissipation rate inside Mimas. In this 'hot Mimas' scenario, we assume that melting runaway and abrupt increase of dissipation in Mimas occur when the eccentricity exceeds a critical value, typically varying between 0.18 and 0.22. This maximal eccentricity controls the range of orbital recession of Mimas, see Fig. 2. The dissipation function of Mimas (k_2/Q) typically varies between 10^{-7} and 10^{-6} before melting occurs, and between 10^{-4} and 10^{-2} once a liquid layer forms, depending on the ocean/ice thickness and the effective viscosity/strength of the rocky core and outer ice shell, (Appendix A).

6.1 Analytical model

While Mimas and Tethys are locked in the 2: 1 resonance, the equations (15), (16), (17), and (28), which determine their long-term orbital motions, become

$$\left\langle \frac{\mathrm{d}n_1}{\mathrm{d}t} \right\rangle = 3n_1^2\alpha_{13}\frac{m_3}{M_Y} < e_1 f(\alpha_{13}) \sin\phi_1 > + \left(\frac{\mathrm{d}n_1}{\mathrm{d}t}\right)_T + \left(\frac{\mathrm{d}n_1}{\mathrm{d}t}\right)_R, \tag{32}$$

$$\left\langle \frac{\mathrm{d}n_3}{\mathrm{d}t} \right\rangle = -6n_3^2\frac{m_1}{M_Y} < e_1 f(\alpha_{13}) \sin\phi_1 > + \left(\frac{\mathrm{d}n_3}{\mathrm{d}t}\right)_T, \tag{33}$$

$$\left\langle \frac{\mathrm{d}e_1}{\mathrm{d}t} \right\rangle = n_1\alpha_{13}\frac{m_3}{M_Y}\frac{< e_1 f(\alpha_{13}) \sin\phi_1 >}{e_1} + \left(\frac{\mathrm{d}e_1}{\mathrm{d}t}\right)_T, \tag{34}$$

$$< e_1 f(\alpha_{13}) \sin\phi_1 >= \frac{2\left(\frac{\mathrm{d}n_3}{\mathrm{d}t}\right)_T - \left[\left(\frac{\mathrm{d}n_1}{\mathrm{d}t}\right)_T + \left(\frac{\mathrm{d}n_1}{\mathrm{d}t}\right)_R\right]}{3n_1^2\alpha_{13}\frac{m_3}{M_Y} + 12n_3^2\frac{m_1}{M_Y}}. \tag{35}$$

Fig. 1 gives an example of trajectory of Mimas in this scenario. We took $(k_2/Q)_Y = 1.59 \times 10^{-4}$, an initial semimajor axis of Tethys $a_3 = 284\,000$ km, no dissipation in Tethys, i.e. $(k_2/Q)_3 = 0$, and $(k_2/Q)_1 = 10^{-7}$ before the eccentricity of 0.22 is reached, $(k_2/Q)_1 = 10^{-3}$ after, and $(k_2/Q)_1 = 1.227 \times 10^{-6}$ at the end, so as to maintain the current eccentricity of Mimas. Here the capture into the present inclination resonance with Tethys is not simulated. The trapping into the 2: 1 e-resonance with Tethys occurs at ≈46 Myr, from which the evolution of the orbital elements of Mimas and Tethys is modelled with equations (32)–(35). This resonance is disrupted when the eccentricity of Mimas reaches 0.22, at ≈303.5 Myr.

Once Mimas' interior starts melting, the internal dissipation rapidly increases, leading to a disruption of the resonance and to an inward migration. A critical point is the length of Mimas' recession, i.e. the Δa, which is the difference in semimajor axis between its maximum, at the beginning of the inward migration phase, and its minimum, when the migration is reversed. This recession can be analytically estimated.

From the equations of the secular evolution of the orbit of Mimas due to the tides and the rings (equations 1, 3, and 4), we can write

$$\frac{\mathrm{d}a_1}{\mathrm{d}t} = \kappa_0 + \kappa_1 e_1^2, \tag{36}$$

$$e_1(t) = e_0 \exp\left(-\frac{t}{\tau}\right), \tag{37}$$

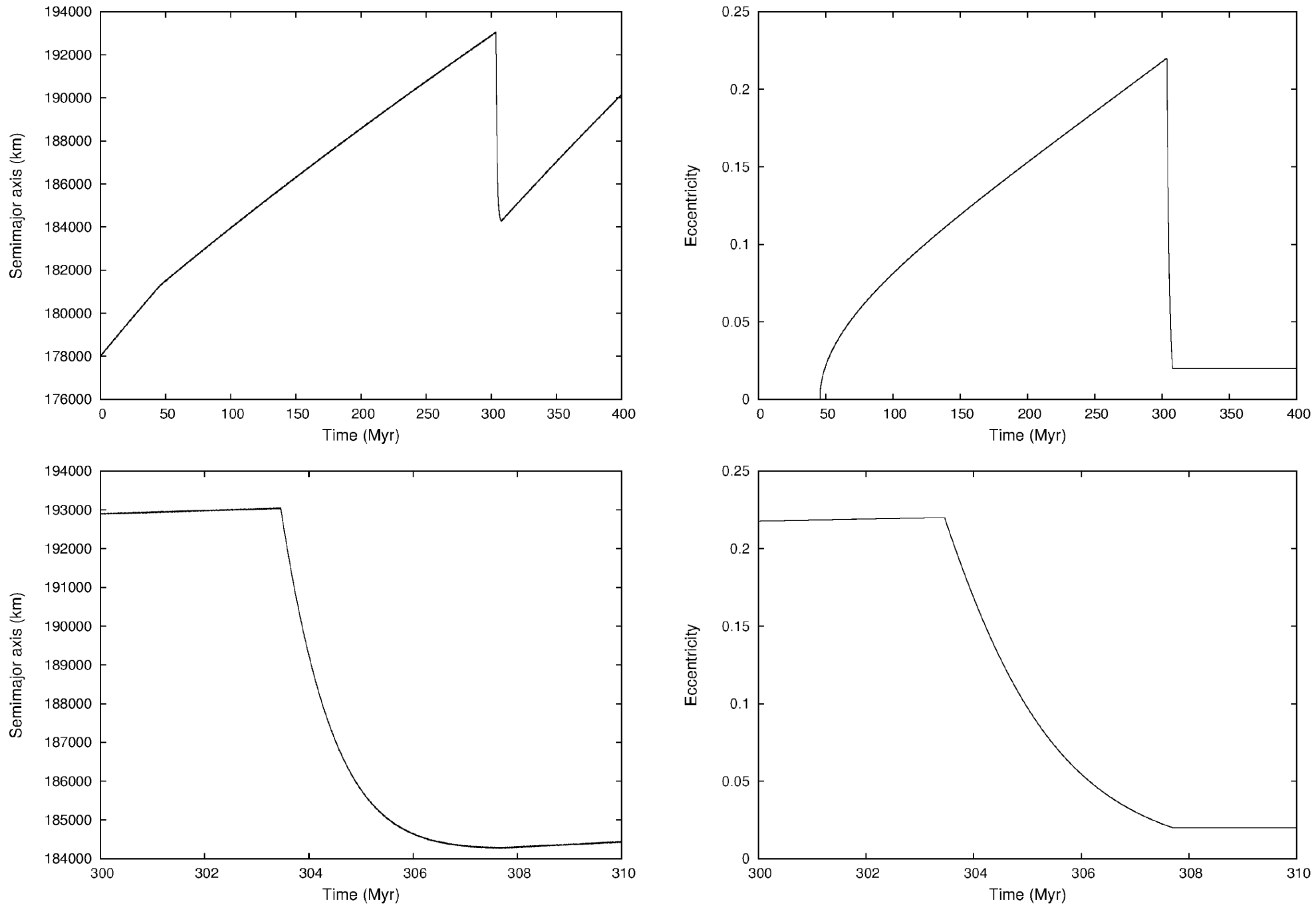

Figure 1. Synthetic evolution of the orbit of Mimas in the Scenario 1, the bottom being a zoom on the inward migration. During a phase of outward migration due to the tides and the push of the rings, Mimas is caught in the 2: 1 e-resonance with Tethys, which triggers a rapid raise of its eccentricity. When this eccentricity reaches 0.2, we consider that Mimas is hot enough to experience an impulsive raise of its (k_2/Q), which disrupts the MMR, triggers the inward migration, and damps its eccentricity. After this phase, Mimas recrystallizes, and resumes its outward migration.

with

$$\kappa_0 = \frac{4}{3}\pi^2\sigma_{2\mathrm{l}} n a^3 \alpha^3 \frac{m_1}{M_Y}\left(4b_{1/2}^{(2)}(\alpha) + \alpha\frac{\mathrm{d}b_{1/2}^{(2)}}{\mathrm{d}\alpha}(\alpha)\right)^2 + 3\left(\frac{k_2}{Q}\right)_Y n\frac{m_1}{M_Y}\frac{R_Y^5}{a^4}, \tag{38}$$

$$\kappa_1 = \frac{153}{4}\left(\frac{k_2}{Q}\right)_Y n\frac{m_1}{M_Y}\frac{R_Y^5}{a^4} - 21\left(\frac{k_2}{Q}\right)_1 n\frac{M_Y}{m_1}\frac{R_1^5}{a^4}, \tag{39}$$

$$\tau = \left(n\left(\frac{21}{2}\left(\frac{k_2}{Q}\right)_1\frac{M_Y}{m_1}\left(\frac{R_1}{a}\right)^5 - \frac{57}{8}\left(\frac{k_2}{Q}\right)_Y\frac{m_1}{M_Y}\left(\frac{R_Y}{a}\right)^5\right)\right)^{-1}, \tag{40}$$

in which the mean motion and semimajor axis of Mimas are fixed to constant values $n = 6.269\ \mathrm{rad\,d^{-1}}$ and $a = 190\,000$ km, given their relative small range of variation. Moreover, we took $\sigma_{2:1} = 28.6\ \mathrm{g\,cm^{-2}}$ from our model of initial ring (cf. Paper I).

The duration of the recession phase t_d is the time for which $\mathrm{d}a_1/\mathrm{d}t = 0$, i.e.

$$t_\mathrm{d} = -\frac{\tau}{2}\ln\left(-\frac{\kappa_0}{\kappa_1 e_0^2}\right), \tag{41}$$

and the length of the inward migration Δa reads:

$$\Delta a = \kappa_0 t_\mathrm{d} + \frac{\kappa_1}{2}\tau e_0^2\left(1 - \exp\left(-2\frac{t_\mathrm{d}}{\tau}\right)\right). \tag{42}$$

These quantities are represented in Fig. 2. We aim at migrating inwards over at least 8000 km, which would imply a maximal eccentricity $e_0 = 0.208$ for $(k_2/Q)_1 = 2\times10^{-3}$, and $e_0 = 0.225$ for $(k_2/Q)_1 = 2\times10^{-4}$.

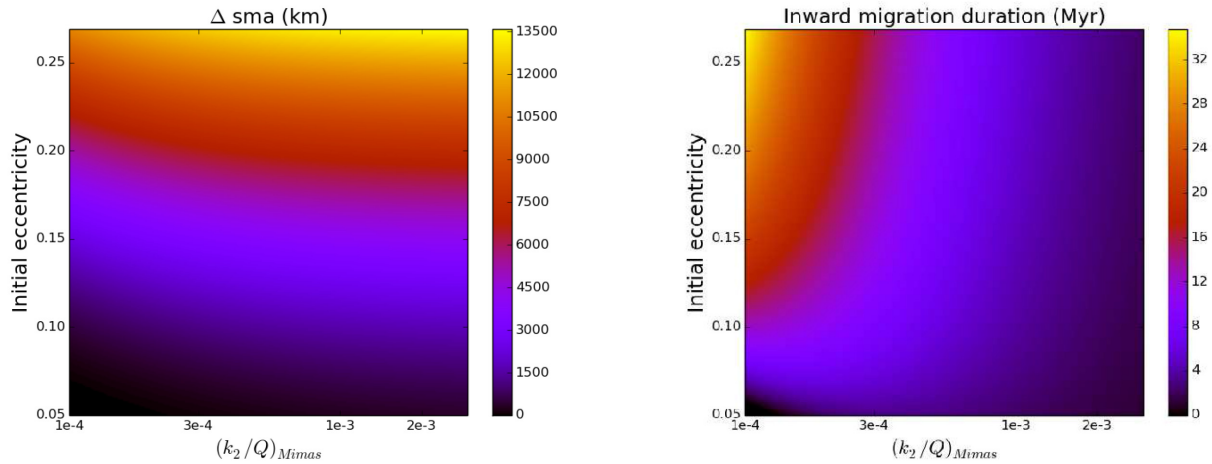

Figure 2. Length (left) and duration (right) of the orbital recession of Mimas, with respect to its dissipation and initial eccentricity.

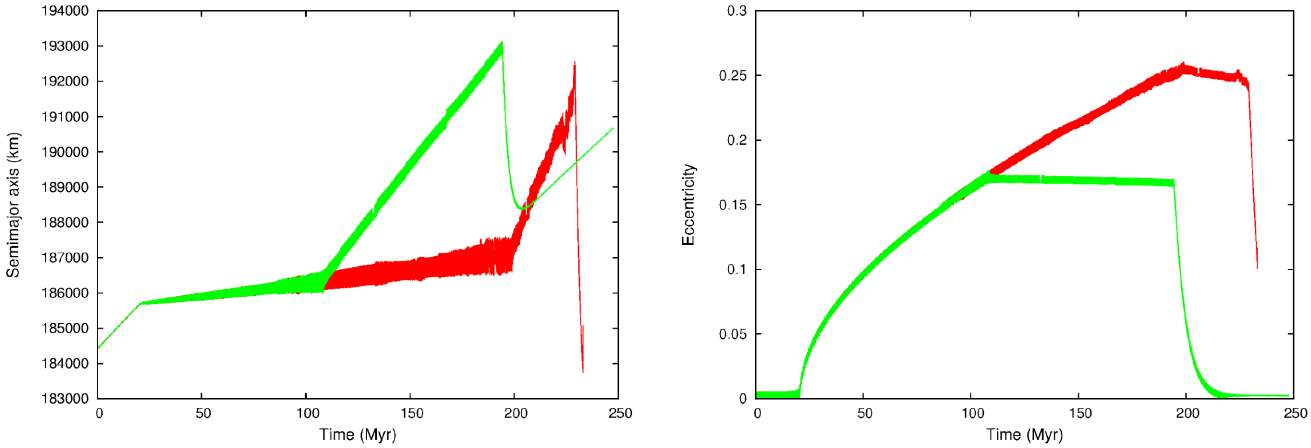

Figure 3. Two examples of orbital evolution of Mimas, with very close initial conditions, from *N*-body simulations. The chaoticity of the real system when Mimas attains a significant eccentricity makes the stability of the MMR between Mimas and Tethys impossible to control, which is why several simulations are necessary. When the eccentricity gets too high (red curve), the inward migration is so abrupt that the simulation becomes numerically unstable.

6.2 Numerical validation

We ran more than 100 *N*-body simulations, and in all of them Mimas and Tethys were trapped into the e-resonance we mentioned, provided the numerical simulations were not accelerated too much. We tested the influence of the acceleration on the trapping into resonance, and it appeared that an acceleration by a factor 50 000 remains slow enough to have a certain capture. This acceleraton is obtained by multiplying the tidal coefficients (k_2/Q) by 50 000. However, accelerating the migration by a factor 500 000 prevents the locking into that resonance (Fig. 4) However, the resonance is still certain when the migration is accelerated only by a factor 5000. Our last set of simulations consisted of 10 runs involving six satellites, from Mimas to Titan, which differed by the initial mean anomaly of Mimas. We got a trapping in all of these simulations. However, they differ by the disruption of this resonance (Fig. 3). We conjecture that slower simulations would give the same behaviours over a set of simulations. Unfortunately, the chaoticity of the problem, especially when Mimas reaches high eccentricities, prevents two simulations differing only by the acceleration factor to result in the same trajectory. The trapping into the e-resonance with Tethys is preserved, however the disruption of this resonance cannot be accurately constrained by *N*-body simulations (Fig. 4). The increase of $(k_2/Q)_1$ is based on the semimajor axis instead of being based on the eccentricity as it would be physically relevant. This way, we initiate the orbital decay where the Paper I predicts it.

Fig. 3 shows two trajectories. In the first one, the resonance is disrupted for $e \approx 0.17$, which gives an inward migration over ≈4500 km. However, the second trajectory maintains the resonance until $e = 0.25$, which induces such an abrupt inward migration that it challenges the numerical accuracy of our code. In both cases, the dissipative Love number of Mimas $(k_2/Q)_1$ is abruptly raised when the semimajor axis of Mimas reaches 193 150 km. As further explained in Section 6.3 and in Appendix A, the abrupt rise of $(k_2/Q)_1$ is explained by a melting runaway event. Such an event is triggered when the eccentricity and hence the tidal heating reach a critical value. In reality, the associated $(k_2/Q)_1$ rise is not instantaneous and should proceed on a time-scale of a few hundred thousands of years. As this time-scale is relatively short compared to the orbital evolution, we simplify it by considering an abrupt instantaneous jump in $(k_2/Q)_1$.

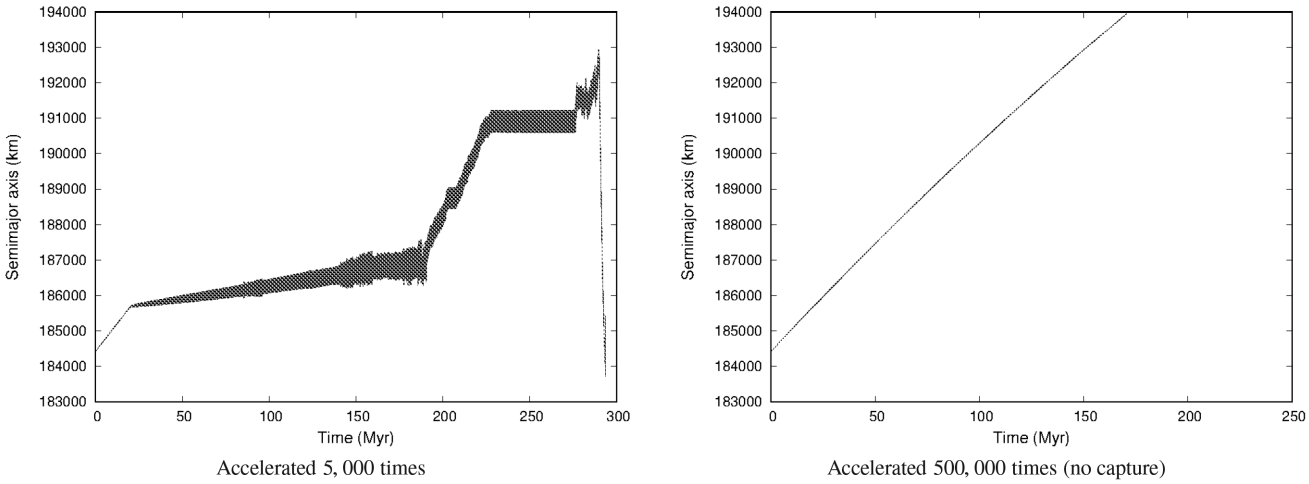

Figure 4. Influence of the artificial acceleration of the tidal migration on the simulated orbital evolution of Mimas. Accelerating it 5000 times (left) does not give exactly the same trajectories as 50 000 (Fig. 3, left, green curve), but renders the trapping into the e-resonance and the raise of the eccentricity. However, accelerating it 500 000 times (right) prevents the trapping into the resonance, the evolution is not adiabatic anymore.

6.3 Origin of the $(k_2/Q)_1$ increase and thermal implications

In the proposed scenario, the abrupt change of $(k_2/Q)_1$ when the eccentricity exceeds a critical value (0.22 in the example shown in Fig. 1) is related to the melting of the icy interior of Mimas. This runaway melting leads to the formation of an internal ocean and hence to a strong increase of interior deformation in response to tides raised by Saturn. Using the approach of Tobie, Mocquet & Sotin (2005), we determined the possible values of $(k_2/Q)_1$ assuming various interior structures. The interior is assumed to behave as a Maxwellian body and to be differentiated into a rock-rich core (consisting of a mixture of rock and ice or rock and liquid water) and an ice shell, possibly separated by a liquid water layer, with various thickness (see Appendix A for further details). Our calculations show that values of $(k_2/Q)_1$ lower than 10^{-6} are predicted for fully solid body consisting of a rock-ice core overlaid by a thick ice mantle with average viscosity larger than 10^{17} Pa.s, while values higher or equal to 10^{-3} correspond to an interior model consisting of a porous water-filled core overlaid by a thick ocean and ice shell. The abrupt change can be understood as the consequence of a melting runaway that occurs once the melting point was reached in the icy interior.

The total dissipated power, $P_{\rm tide}$, can be estimated using the following formula (e.g. Tobie et al. 2005):

$$P_{\rm tide} = \frac{21}{2}\frac{k_2}{Q}\frac{(\omega R_s)^5}{\mathcal{G}}e^2, \tag{43}$$

where ω is the rotational frequency of the satellite, usually assumed to be equal to the mean motion n.

At an eccentricity equal to 0.22, the total dissipated power rapidly jumps from 0.6 GW for $(k_2/Q)_1 = 10^{-7}$ to 6 TW for $(k_2/Q)_1 = 10^{-3}$ when melting would first occur. As long as the eccentricity is low, the heat rate is too low to significantly increase the internal temperature. But once temperature reaches the melting point in the interior, $(k_2/Q)_1$ is expected to increase leading to an enhancement of heat rate and hence to more melting. The total energy required to melt the ice phase of Mimas is estimated to be about 10^{25} J, implying that the entire ice phase would be melted in about 300 kyr at a rate of 1 TW.

Our simulation shows that the orbital recession of Mimas over a distance of 8000–9000 km requires Mimas to remain in a highly dissipative state during at least 3 Myr (Simulation 2 in Paper I). This implies that Mimas would be in a fully molten state during this entire period, with only a very thin ice shell (<1 km) which is incompatible with its highly cratered surface, showing no sign of significant past tectonic activity (e.g. Rhoden et al. 2017). Even though we show that a highly dissipative state can be reached when Mimas started melting, the duration over which such dissipation must act to proceed the required orbital decay and the lack of significant tectonic activity strongly constrain a scenario of hot Mimas.

7 SCENARIO II: FROM A HOT ENCELADUS

Mimas does not show evidence of a past heating as intense as expected from Scenario 1. However, Enceladus shows intense activity at present (e.g. Porco et al. 2006; Spencer et al. 2006), which may have been even higher in the past (e.g. Běhounková et al. 2012). In particular, several ancient tectonized terrains have been identified outside the active south polar terrains (Crow-Willard & Pappalardo 2015), suggesting significant variations in surface activity and internal dissipation. This prompts us to examine the following scenario:

(i) Enceladus attains a high eccentricity, which triggers an episode of intense dissipation and inward migration,

(ii) While it migrates inwards, it traps Mimas into a mean-motion resonance, and they both migrate inwards. The stability of this resonance is enforced by the convergence of the two orbits when the resonance occurs, but could be threatened by a trapping into another resonance.

Table 1. Orbital elements of the mid-sized satellites of Saturn. These are mean elements given by JPL HORIZONS, except for the eccentricity of Enceladus, which is given as 0 since it is its free component. Its typical instantaneous value is more relevant.

Satellite	Semimajor axis (km)	Eccentricity	Inclination
S-1 Mimas	185 539	1.96×10^{-2}	1.574°
S-2 Enceladus	238 042	5×10^{-3}	0.003°
S-3 Tethys	294 672	10^{-4}	1.091°
S-4 Dione	377 415	2.2×10^{-3}	0.028°

Table 2. Semimajor axes of some small, inner satellites of Saturn. These are mean elements given by JPL HORIZONS.

Satellite	Semimajor axis (km)	Eccentricity
S-10 Janus	151 450	9.8×10^{-3}
S-11 Epimetheus	151 450	1.61×10^{-2}
S-15 Atlas	137 774	1.1×10^{-3}
S-16 Prometheus	139 429	2.2×10^{-3}
S-17 Pandora	141 810	4.2×10^{-3}
S-18 Pan	133 585	0
S-32 Methone	194 402	0
S-33 Pallene	212 282	4×10^{-3}
S-49 Anthe	196 888	1.1×10^{-3}
S-53 Aegaeon	167 425	2×10^{-4}

Table 3. Gravity field (Jacobson et al. 2006) and radii (Thomas et al. 2007; Thomas 2010) of Saturn and its mid-sized satellites used in our simulations.

	$\mathcal{G}M$ ($km^3.s^{-2}$)	Mean radius (km)
Saturn	37 931 272	58 232
Mimas	2.5023	198.2
Enceladus	7.2096	252.1
Tethys	41.2097	531
Dione	73.1127	561.4
Saturn		
Equatorial radius	60 330 km	
J_2	1.629071×10^{-2}	
J_4	-9.3583×10^{-4}	
J_6	8.614×10^{-5}	

Table 4. Constraints on the past motion of Enceladus in Scenario 2, with respect to the resonance involved.

Resonance	3 : 2	4 : 3
Argument	$\phi_{32} = 2\lambda_1 - 3\lambda_2 + \varpi_2$	$\phi_{43} = 3\lambda_1 - 4\lambda_2 + \varpi_2$
$\alpha = a_1/a_2$	0.76337	0.82564
Capture sma	253 029 km	233 939 km
Release sma	242 347 km	224 067 km
Required migration	10 676 km	9871 km

(iii) The eccentricity of Enceladus is then damped enough so that the inward migration is stopped. The mean-motion resonance with Mimas is disrupted, and the two bodies migrate outwards independently. Mimas is eventually trapped into its present 4 : 2 MMR with Tethys, while Enceladus is trapped into the 2 : 1 MMR with Dione.

The two strongest candidates for the MMR between Mimas and Enceladus are the 3 : 2 and the 4 : 3 ones. We compare their effects in Table 4.

The capture semimajor axis is the semimajor axis where Enceladus would have been trapped into MMR with Mimas, if Mimas started its inward migration at 193 150 km. The release semimajor axis is the one of Enceladus at the disruption of the resonance, if it would have happened when Mimas was at 185 000 km. These numbers are to be compared with the current mean semimajor axis of Enceladus, which is

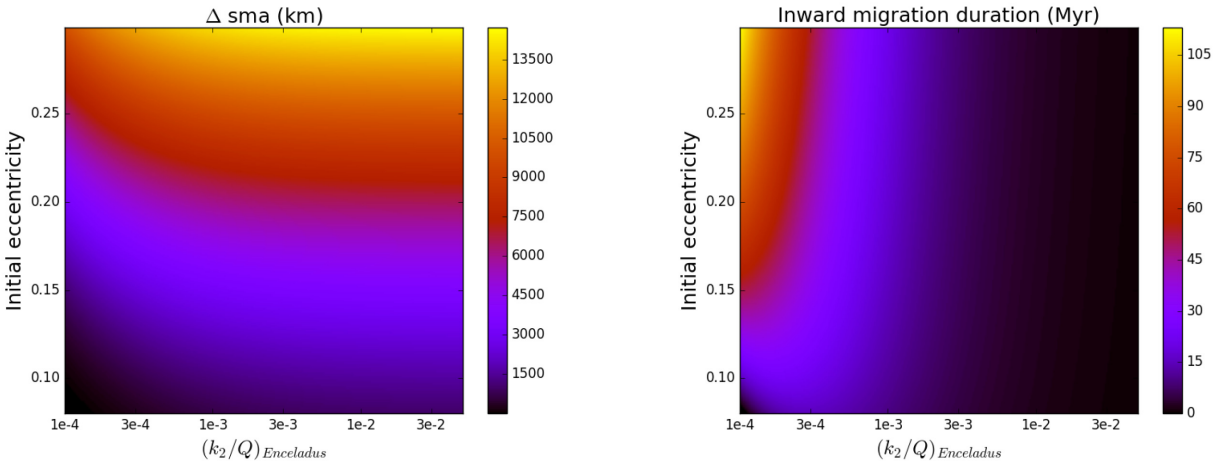

Figure 5. Length (left) and duration (right) of the orbital recession of Enceladus, with respect to its dissipation and its initial eccentricity.

238 042 km. This means that if the system was trapped into the 3 : 2 MMR, then an extra inward migration would have been needed to drive the semimajor axis of Enceladus below its current value, and then outward migration would have started to get Enceladus trapped into the current MMR with Dione. This extra migration would not have been needed for the 4 : 3 MMR, but it would have required a fast outward migration instead, Enceladus moving from 224 000 to 238 000 km while Mimas would have moved from 185 000 to 185 500 km.

Deriving the decay range of Enceladus should consider that the dissipated energy into Enceladus would translate into the inward migration of Enceladus and of Mimas. This dissipated energy should read as:

$$\begin{aligned}\Delta E &= \frac{\mathcal{G}M_Y m_2}{2a_2^2}\Delta a_2 + \frac{\mathcal{G}M_Y m_1}{2a_1^2}\Delta a_1 \\ &= \frac{\mathcal{G}M_Y}{2a_2^2}\Delta a_2\left(m_2 + \frac{m_1}{\alpha}\right),\end{aligned} \tag{44}$$

which means that the length of the migration, if calculated for Enceladus alone, should be multiplied by $m_2/(m_2 + m_1/\alpha)$. This factor is equal to 0.687 for the 3 : 2 MMR, and to 0.704 for the 4 : 3 MMR. This migration is represented in Fig. 5, for the 3 : 2 MMR.

This figure shows in particular that the required migration associated with the 3 : 2 MMR, i.e. 10 676 km, would require an initial eccentricity $e_2 = 0.294$ for $(k_2/Q)_2 = 10^{-4}$, and $e_2 = 0.258$ for $(k_2/Q)_2 = 2 \times 10^{-3}$. For the 4 : 3 MMR, which would require an inward migration over 9871 km, an initial eccentricity $e_2 = 0.291$ would be needed for $(k_2/Q)_2 = 10^{-4}$, and $e_2 = 0.246$ for $(k_2/Q)_2 = 2 \times 10^{-3}$.

For an initial $e_2 = 0.25$ and $(k_2/Q)_2 = 2 \times 10^{-3}$ we obtain an orbital decay over 9659 km. This is actually an optimistic estimate, since it does not consider the push of the rings and of the tides of Saturn on Mimas. To check this number, we simulated secular resonant trajectories. If Mimas and Enceladus are trapped into the 3 : 2 MMR, the equations (15), (16), (18), and (28) become, with $p = 2$, $q = q_2 = 1$, and $q_1 = q_3 = q_4 = 0$:

$$\left\langle \frac{\mathrm{d}n_1}{\mathrm{d}t} \right\rangle = 6n_1^2\alpha_{12}\frac{m_2}{M_Y} < e_2 f(\alpha_{12})\sin\phi_{32} > + \left(\frac{\mathrm{d}n_1}{\mathrm{d}t}\right)_T + \left(\frac{\mathrm{d}n_1}{\mathrm{d}t}\right)_R, \tag{45}$$

$$\left\langle \frac{\mathrm{d}n_2}{\mathrm{d}t} \right\rangle = -9n_2^2\frac{m_1}{M_Y} < e_2 f(\alpha_{12})\sin\phi_{32} > + \left(\frac{\mathrm{d}n_2}{\mathrm{d}t}\right)_T, \tag{46}$$

$$\left\langle \frac{\mathrm{d}e_2}{\mathrm{d}t} \right\rangle = n_2\frac{m_1}{M_Y}\frac{< e_2 f(\alpha_{12})\sin\phi_{32} >}{e_2} + \left(\frac{\mathrm{d}e_2}{\mathrm{d}t}\right)_T, \tag{47}$$

$$< e_2 f(\alpha_{12})\sin\phi_{32} >= \frac{3\left(\frac{\mathrm{d}n_2}{\mathrm{d}t}\right)_T - 2\left[\left(\frac{\mathrm{d}n_1}{\mathrm{d}t}\right)_T + \left(\frac{\mathrm{d}n_1}{\mathrm{d}t}\right)_R\right]}{12n_1^2\alpha_{12}\frac{m_2}{M_Y} + 27n_2^2\frac{m_1}{M_Y}} \tag{48}$$

and the simulation of the trajectory gives a migration of ≈8900 km instead of 9659 km, which was obtained with optimistic assumptions. This means that the initial eccentricity given by Fig. 5 should be slightly raised to be realistic.

7.1 Numerical limits

If the migration of Mimas had been due to the migration of a hot, dissipating Enceladus, it would have required its eccentricity to reach at least 0.25, which is extremely high for a natural satellite. Such an eccentricity could threaten the very stability of part of the system, i.e. the presence of Enceladus around Saturn, and/or the survival of smaller satellites.

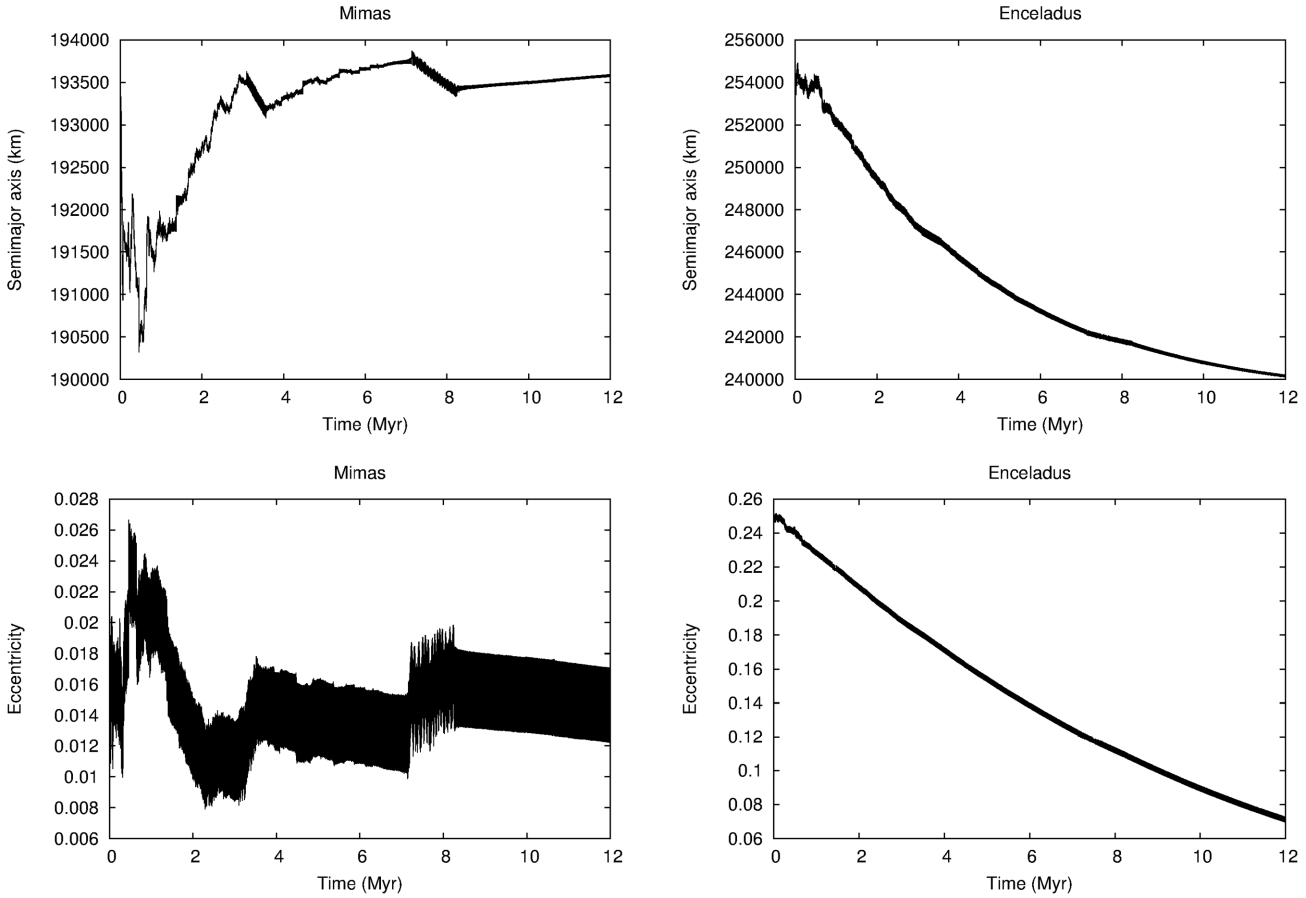

Figure 6. Scenario 2, with Mimas and Enceladus initially close to the 3 : 2 MMR, and Dione perturbing them. Mimas experiences two episodic captures into the 3 : 2 and the 4 : 3 MMR, but which are too unstable to permit an inward migration over more than 8000 km, as wished to create the Cassini Division.

We have run 10 numerical simulations close to the 3 : 2 MMR, with only three bodies, i.e. Mimas, Enceladus, and Dione (cf. example Fig. 6), with the tides accelerated 5000 times, and with an initial eccentricity of Enceladus of 0.25. It appeared that in none of them, the 3 : 2 MMR is stable enough to drive Mimas closer to Saturn. Actually, the migration of the satellites is dominated by the chaotic interaction between them.

In some of our trajectories, we get temporary trappings into the 4 : 3 MMR (cf. Fig. 6, between 4 and 7 Myr), indicating that this resonance is more stable. We ran 10 simulations with the same three bodies and Mimas–Enceladus close to the 4 : 3 MMR, and in five of them we got the desired-for migration for Mimas, unfortunately over a range of up to ≈2000 km only. Moreover, this process does not survive the gravitational interactions with the other bodies, i.e. the system of the mid-sized satellites of Saturn becomes unstable. We ran 20 simulations close to the 4 : 3 MMR, in which the first six satellites were considered, i.e. from S-1 Mimas to S-6 Titan. In none of them, the process works, and usually the trajectory becomes quickly unstable (cf. Fig. 7).

Many other MMR could be considered, but they would be much weaker since there are higher order resonances. We tried the same three-body simulations with Mimas and Enceladus close to the 7 : 5 MMR, with no success.

7.2 Thermal implications

Like in the 'hot Mimas' scenario, the 'hot Enceladus' scenario implies an abrupt change in dissipation inside Enceladus. This occurs again when a global ocean is generated by ice melting. When the eccentricity of Enceladus exceeds a critical value, estimated to be about 0.25 in our scenario, an episode of intense dissipation is triggered, leading to inward migration. As Mimas is trapped into a mean-motion resonance, it is dragged inwards by Enceladus. Our calculations (equation 44) show that an orbital regression of Mimas over a distance of 8000–9000 km requires a total energy of 4.8×10^{26} J to be dissipated inside Enceladus. Like in the hot Mimas scenario, this would imply an almost complete melting of the internal ice. At present, Enceladus' ice shell thickness is estimated to about 20–25 km on average (Thomas et al. 2016), with thickness as small as 2–4 km in the south polar region (Beuthe et al. 2016; Čadek et al. 2016). During periods of intense dissipation, the ice shell could be even thinner, especially in the south polar terrain as well as in other area outside the south polar region where highly tectonized terrains have been identified (Crow-Willard & Pappalardo 2015). In very thin and highly deformable regions, the surface heat flux could exceed several tens of $W\,m^{-2}$, providing a means to evacuate the excess of dissipated heat. During periods of high eccentricity, the tidal

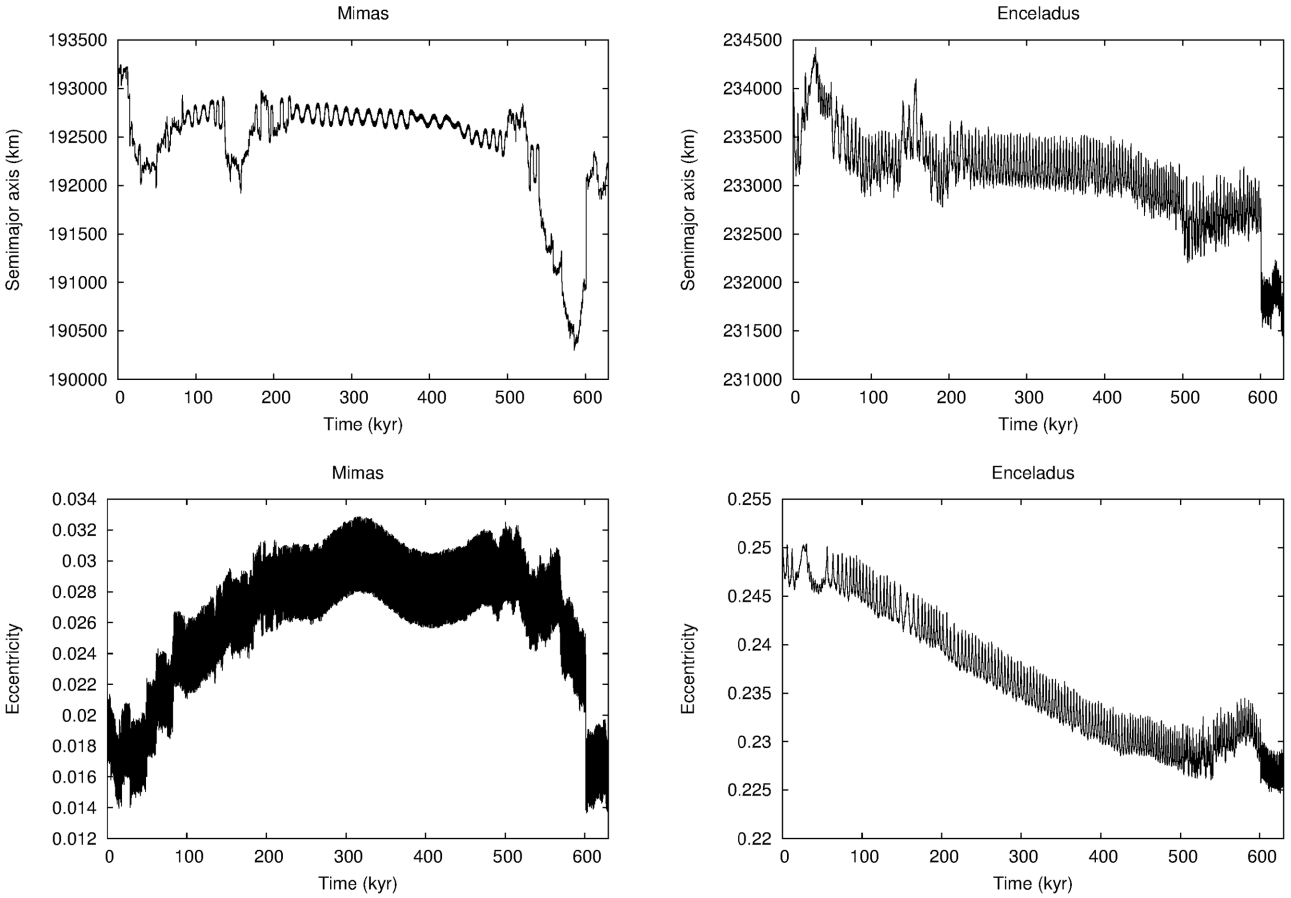

Figure 7. Scenario 2, with Mimas and Enceladus initially close to the 4: 3 MMR. Six satellites are present in this simulation. When Enceladus has such a significant eccentricity, the system of the satellites of Saturn is destabilized, which is why all the simulations are stopped before 1 Myr.

deformation will be very large especially in regions with reduced ice thickness (Souček et al. 2016), which is expected to lead to a break-up of the ice shell and exposure of liquid water on a large fraction of the ice shell. The radiative cooling of erupted water would provide an efficient way to release the dissipated heat. For water/ice mixture exposed at the surface at temperature between 200 and 270 K, the radiative cooling heat flux is estimated between 90 and 300 W m^{-2}. Less than 5 per cent of the surface of Enceladus with such a surface activity would be sufficient to release 3–4 TW. This indicates that a period with a very intense dissipation exceeding 1 TW is possible on Enceladus and is not incompatible with its surface activity. However, as mentioned above, a highly eccentric orbit for Enceladus challenges the stability of the orbits of the other satellites.

8 SURVIVAL OF THE OTHER SATELLITES

Pumping the eccentricity of Mimas or Enceladus might threaten the existence of small satellites in case of collision, and the stability of the system of Saturn if larger satellites were affected. Table 5 presents the maximal eccentricities Mimas and Enceladus could have while preserving the existence of the satellites listed in the first column. For Mimas and Enceladus, two semimajor axes were considered: a location slightly closer than the present one, and the maximal one predicted by our study. We give these two locations to cover the full putative excursions of the satellites, but large eccentricities are more relevant for the highest of these semimajor axes, where the inward migration starts.

We derived the minimum distance D between two orbits as the distance between the pericentre of the outer satellite (2) with the apocentre of the inner one:

$$D = |a_1 - a_2| - a_1 e_1 - a_2 e_2. \tag{49}$$

This formula assumes that there is no resonant interaction between the two orbits, and that the orbits are coplanar. This last assumption is reasonable since only Mimas and Tethys have significant inclinations, and the one of Mimas is assumed to be younger than the Cassini Division. So, the result could be slightly pessimistic for Tethys. Then this mininum distance D should be compared to $2.2R_H$, R_H being the

Table 5. Maximal eccentricities of Mimas and Enceladus at different locations to avoid collisions with the existing other satellites. These numbers should be compared with 0.22 in the hot Mimas scenario, and with 0.25 in the hot Enceladus one.

	Mimas 185 000 km	Mimas 194 000 km (hot Mimas)	Enceladus 238 000 km	Enceladus 248 000 km (hot Enceladus)
Aegaeon	0.089	0.131	0.289	0.317
Janus	0.168	0.206	0.350	0.376
Epimetheus	0.163	0.201	0.346	0.372
Pandora	0.225	0.260	0.395	0.419
Prometheus	0.239	0.274	0.406	0.430
Atlas	0.249	0.284	0.414	0.437
Pan	0.273	0.306	0.432	0.455
Methone	0.045	0	0.175	0.208
Anthe	0.057	0.008	0.164	0.197
Pallene	0.136	0.083	0.096	0.132
Mimas	–	–	0.196	0.229
Enceladus	0.269	0.210	–	–
Tethys	0.572	0.499	0.219	0.170

Hill radius of the two satellites, with

$$R_{\rm H} = \frac{a_1 + a_2}{2} \left(\frac{m_1 + m_2}{3 M_Y} \right)^{1/3}. \tag{50}$$

8.1 Stability of the inner satellites

The scenario of a hot Mimas leaves no chance to Aegaeon and threatens the existence of Janus and Epimetheus, since an eccentricity of 0.21 would be high enough to destabilize them, unless trapped in mean-motion resonance with Mimas. However, Pandora, Prometheus, Atlas, and Pan would probably be preserved. Nevertheless, this calculation does not consider the orbital perturbations that a highly eccentric Mimas would induce on these bodies. However, the scenario of a hot Enceladus preserves all of these bodies.

8.2 Stability of the Alkyonides

The very small satellites Methone, Pallene, and Anthe would not have survived either of these scenarios if they were not trapped in mean-motion resonances. Anyway, a significant past eccentricity of Mimas or Enceladus raises questions about their origin. Either they are younger than 10 Myr, or the MMR survived that episode. Answering this question would require a dedicated study.

The stability of these bodies has recently been addressed in Munõz-Gutiérrez & Giuliatti Winter (2017) over the last 500 kyr, the authors have particularly shown that the mean-motion resonances do play a compelling role in this issue.

8.3 Stability of the system of Saturn

Close encounters between two massive satellites may threaten the very existence of the system as presently observed. And it appears that a significant increase of the eccentricity of Enceladus is very likely to induce a collision with Tethys, while a high eccentricity of Mimas could provoke a collision with Enceladus, though less certain.

9 CONCLUSIONS

In this paper, we investigated two a priori possible explanations for a past episode of inward migration of Mimas: an intense past heating of Mimas, and an intense past heating of Enceladus. Both scenarios have pros and cons. The scenario of a hot Mimas preserves the structure of the system of the mid-sized satellites of Saturn, but threatens the existence of Janus and Epimetheus and implies a past melting of the surface of Mimas, which is hardly consistent with the observations of impact basins by Cassini (e.g. Roatsch et al. 2009, 2013). However, the scenario of a hot Enceladus could be supported by our knowledge of the interior of Enceladus, but would have destabilized the system of the mid-sized satellites. None of these scenarios preserves the small satellites of the Alkyonides group unless trapped in MMR. Another explanation would be that they are younger than 10 Myr.

Despite our difficulties in finding a self-consistent scenario, we believe that the assumption of a past inwardly migrating Mimas should be kept in mind, since no alternative explanation in the literature explains the finite size of the Cassini Division. The two scenarios we

investigated are actually two end-members of a process combining both, i.e. dissipation in Enceladus and in Mimas. We hope that further theoretical studies and data would permit to improve this explanation and/or elaborate a better one.

We could expect future improvements at least in the accuracy of the response of the rings, and in the tidal response of the satellites. The interaction of dense rings with a massive satellite is a non-linear problem, and its determination is still challenging when the perturber is eccentric. Realistic simulations of the behaviour of dense rings with an *N*-body code are still unreachable by classical computation facilities, while the response of a collisional ring as a viscous gas is still modelled under assumptions of small perturbation.

The response of the satellites to tidal excitation could be improved with a better knowledge of their interior, and a better modelling of tides. This topic is still under development. For instance, Renaud & Henning (2018) recently published a new tidal model, using the Sundberg–Cooper rheology, which suggests that the dissipation in icy satellites is currently underestimated.

Since we have two scenarios explaining part of the observed reality, we could expect that a combination of both of them, involving a moderate heating of Mimas and a limited elevation of the eccentricity of Enceladus, would improve the model. Fine-tuning the combination of these two mechanisms would require a whole study.

ACKNOWLEDGEMENTS

BN acknowledges support of the contract Prodex CR90253 from the Belgian Science Policy Office (BELSPO), and KB of the Conseil Scientifique de l'Observatoire de Paris and the Centre National d'Études Spatiales (CNES). VL's research was supported by an appointment to the NASA Postdoctoral Program at the NASA Jet Propulsion Laboratory, California Institute of Technology, administered by Universities Space Research Association under contract with NASA. This study is part of the activities of the ISSI Team *The ENCELADE Team: Constraining the Dynamical Timescale and Internal Processes of the Saturn and Jupiter Systems from Astrometry*. Computational resources have been provided by the Consortium des Équipements de Calcul Intensif (CÉCI), funded by the Fonds de la Recherche Scientifique de Belgique (F.R.S.-FNRS) under Grant No. 2.5020.11. We also thank the referee for detailed and constructive comments that improved the quality of the paper.

REFERENCES

Allan R. R., 1969, AJ, 74, 497
Baillié K., Colwell J. E., Lissauer J. J., Esposito L. W., Sremčević M., 2011, Icarus, 216, 292
Baillié K., Colwell J. E., Esposito L. W., Lewis M. C., 2013, AJ, 145, 171
Baillié K., Noyelles B., Lainey V., Charnoz S., Tobie G., 2019, MNRAS, Formation of the Cassini Division – I. Shaping the rings by Mimas inward migration.
Běhounková M., Tobie G., Choblet G., Čadek O., 2012, Icarus, 219, 655
Beuthe M., Rivoldini A., Trinh A., 2016, Geophys. Res. Lett., 43, 10088
Bland M. T., Singer K. N., McKinnon W. B., Schenk P. M., 2012, Geophys. Res. Lett., 39, L17204
Buratti B. J., Faulk S. P., Mosher J., Baines K. H., Brown R. H., Clark R. N., Nicholson P. D., 2011, Icarus, 214, 534
Caudal G., 2017, Icarus, 286, 280
Champenois S., 1998, PhD dissertation, Paris Observatory
Choblet G., Tobie G., Sotin C., Běhounková M., Čadek C., Postberg F., Souček O., 2017, Nat. Astron., 1, 841
Cooper N. J., Murray C. D., Evans M. W., Beurle K., Jacobson R. A., Porco C. C., 2008, Icarus, 195, 765
Crow-Willard E. N., Pappalardo R. T., 2015, J. Geophys. Res.: Planets, 120, 928
French R. G., Nicholson P. D., 2000, Icarus, 145, 502
Fuller J., Luan J., Quataert E., 2016, MNRAS, 458, 3867
Goldreich P., Tremaine S., 1980, ApJ, 241, 425
Hairer E., Nørsett S. P., Wanner G., 1993, Solving Ordinary Differential Equations – I. Springer, Berlin
Hedman M. M., Nicholson P. D., 2016, Icarus, 279, 109
Hedman M. M., Cooper N. J., Murray C. D., Beurle K., Evans M. W., Tiscareno M. S., Burns J. A., 2010, Icarus, 207, 433
Howett C. J. A., Spencer J. R., Pearl J., Segura M., 2011, J. Geophys. Res., 116, E03003
Jacobson R. A. et al., 2006, AJ, 132, 2520
Kaula W. M., 1962, AJ, 67, 300
Lainey V. et al., 2017, Icarus, 281, 286
Le Gall A. et al., 2017, Nat. Astron., 1, 0063
Levison H. F., Duncan M. J., 1994, Icarus, 108, 18
Meyer J., Wisdom J., 2008, Icarus, 193, 213
Munõz-Gutiérrez M. A., Giuliatti Winter S., 2017, MNRAS, 470, 3750
Noyelles B., 2017, Icarus, 282, 276
Porco C. C. et al., 2006, Science, 311, 1393
Renaud J. P., Henning W. G., 2018, ApJ, 857, 98
Rhoden A. R., Henning W., Hurford T. A., Patthoff D. A., Tajeddine R., 2017, J. Geophys. Res.: Planets, 122, 400
Roatsch T. et al., 2009, Planet. Space Sci., 57, 83
Roatsch T., Kersten E., Hoffmeister A., Wählisch M., Matz K.-D., Porco C. C., 2013, Planet. Space Sci., 77, 118
Roberts J. H., 2015, Icarus, 258, 54
Saito M., 1974, J. Phys. Earth, 22, 123
Souček O., Hron J., Běhounková M., Čadek O., 2016, Geophys. Res. Lett., 43, 7417
Spencer J. R. et al., 2006, Science, 311, 1401

Spitale J. N., Jacobson R. A., Porco C. C., Owen W. M., 2006, AJ, 132, 692
Struve H., 1890, Astron. Nachr., 125, 2983
Tajeddine R., Rambaux N., Lainey V., Charnoz S., Richard A., Rivoldini A., Noyelles B., 2014, Science, 346, 322
Takeuchi H., Saito M., 1972, Methods comput. phys., 11, 217
Thomas P. C. et al., 2007, Icarus, 190, 573
Thomas P. C., 2010, Icarus, 208, 395
Thomas P. C., Tajeddine R., Tiscareno M. S., Burns J. A., Joseph J., Loredo T. J., Helfenstein P., Porco C., 2016, Icarus, 264, 37
Tobie G., Mocquet A., Sotin C., 2005, Icarus, 177, 534
Verheylewegen E., Noyelles B., Lemaitre A., 2013, MNRAS, 435, 1776
Yoder C. F., Peale S. F., 1981, Icarus, 47, 1
Ćuk M., Dones L., Nesvorný D., 2016, ApJ, 820, 97
Čadek O. et al., 2016, Geophys. Res. Lett., 43, 5653

APPENDIX A: COMPUTATION OF MIMAS AND ENCELADUS'S k_2/Q RATIO

To model the tidal response of Mimas' and Enceladus' interiors, we consider interior structures consisting of three main layers from centre to surface: a porous water-saturated unconsolidated core, an ocean, and an ice shell thickness with density and radius summarized in Table A1. A Maxwell rheology is considered, characterized by constant values of elastic modulus, μ_i and μ_c, and viscosity, η_i and η_c for the ice shell and the porous rock core, respectively. Range of explored parameter values are listed in Table A1. The ice shell is assumed to be relatively cold and characterized by a high viscosity, while for the porous core we explored a wide range of viscosity and rigidity, corresponding to a cold mixture of rock and ice for the larger values (e.g. Roberts 2015) to an unconsolidated water-filled porous core for the lowest values (Choblet et al. 2017).

Table A1. Model parameters used to compute the tidal response of Mimas and Enceladus.

Parameter	Symbol (unit)	Mimas	Enceladus
Tidal period	T (d)	0.984	1.37
Satellite mass	M (kg)	3.84×10^{19}	1.08×10^{22}
Surface radius	R_s (km)	198	252
Ice shell thickness	d (km)	5–50	5–50 km
Ice shell density	ρ_i (kg m^{-3})	920	920
Ice shell rigidity	μ_i (GPa)	3.3	3.3
Ice shell viscosity	η_i (Pa.s)	$10^{18}-10^{22}$	$10^{18}-10^{22}$
Ocean density	ρ_o (kg m^{-3})	1007	1007
Core density	ρ_c (kg m^{-3})	2500	2500
Core rigidity	μ_c (GPa)	3–10	3–10
Core viscosity	η_c (Pa.s)	$10^{10}-10^{22}$	$10^{10}-10^{22}$

The viscoelastic deformation under the action of periodic tidal forces is computed following the method of Tobie et al. (2005). The satellite interior is divided in three layers, from the centre to the surface: a weak unconsolidated water-saturated porous core, an inviscid water ocean and a viscoelastic ice shell. For simplicity, each layer is assumed to have constant and uniform densities and mechanical properties (see values above and in Table A1). From these profiles, the Poisson equation and the equations of motion are solved for small perturbations in the frequency domain assuming a compressible viscoelastic rheology. The potential perturbation, associated displacement, and stress are computed as a function of radius by integrating the radial functions associated with the radial and tangential displacements (y_1 and y_3, respectively), the radial and tangential stresses (y_2 and y_4, respectively), and the gravitational potential (y_5), as defined by Takeuchi & Saito (1972) in the elastic equivalent problem. For the deformation of the inviscid water ocean, the static simplified formulation of Saito (1974) is adopted relying on two radial functions, y_5 and y_7. The solution in the solid part (porous core and ice shell) is expressed as the linear combination of three independent solutions, which reduces to two independent solutions in the liquid part. The system of six differential equations is solved by integrating the three independent solutions using a fifth-order Runge–Kutta method with adjustive stepsize control from the centre (r = 0 km) to the surface (r = 252 km) and by applying the appropriate boundary conditions at liquid/solid interface. The complex Love number k_2^C, whose imaginary part is equal to k_2/Q is determined from the complex fifth radial function at the planet surface, $y_5^c(R_s)$.

As shown on Fig. A1, values of k_2/Q lower than 10^{-6} are obtained in the case of Mimas for core viscosity higher than 10^{17} Pa.s in the absence of internal ocean, which is consistent with a mixture of water ice and rock below the melting point of water ice. As the interior is warming up, the viscosity is expected to progressively reduce, leading to a progressive increase of k_2/Q. For core viscosity ranging between 10^{13} and 10^{16} Pa.s, which are typical viscosity values expected for ice-rock mixture at the melting point, the formation of an internal ocean increases only slightly the k_2/Q ratio. The strong amplification of the k_2/Q ratio occurs only once the water ice in the core is fully molten and the core becomes very weak due to the presence of water in the pores. This indicates that once ice melting initiates in the core, the increase of dissipation leads to further melting, which in turn amplifies the dissipation, corresponding to a melting runaway. Enceladus should also

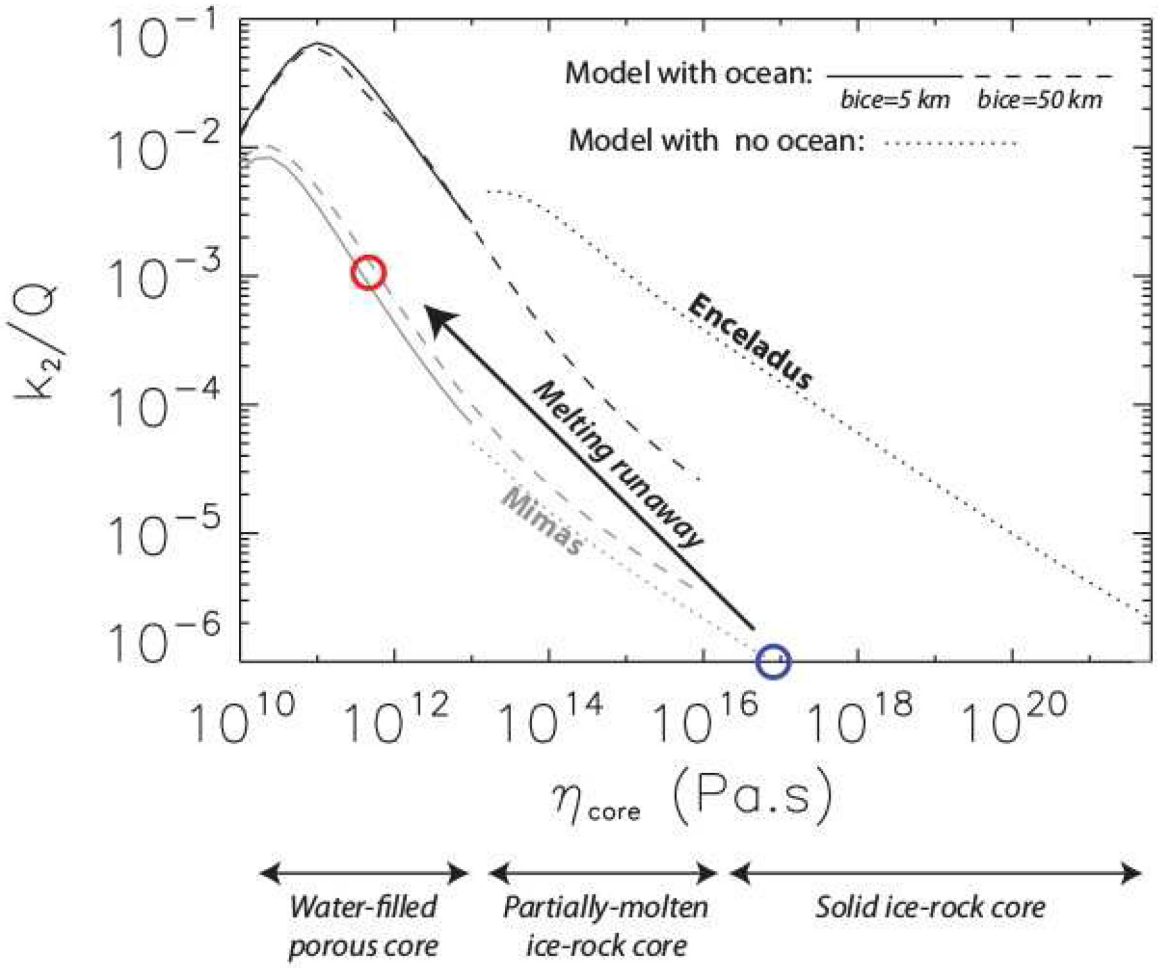

Figure A1. Comparison of k_2/Q ratio computed for Mimas (grey) and Enceladus (black) assuming the same mechanical properties for the interior for models with no ocean (dotted line) and with an ocean beneath an ice shell of 5 km (solid line) or 50 km (dashed line), as a function of the effective core viscosity.

follow a similar trend. Note, however, that in the case of Enceladus, for core viscosities ranging between 10^{14} and 10^{20} Pa.s, the k_2/Q ratio is reduced when the internal ocean is considered. A strong increase of the dissipation for models with ocean compared to the model with no ocean occurs only when the core viscosity gets below 10^{13} Pa.s, corresponding to a full melting of the ice phase. For Enceladus, k_2/Q values potentially as high as 7×10^{-2}, which is about one order of magnitude above the maximal value reached for Mimas. This difference between Mimas and Enceladus is due to the size of the core, which corresponds to about half of the total radius for Mimas, while it is about 3/4 in the case of Enceladus.

This paper has been typeset from a TEX/LATEX file prepared by the author.